Nanoscale

Check for updates

Sunflower pollen-derived microcapsules adsorb light and bacteria for enhanced antimicrobial photothermal therapy†

Yao Yang,‡[a] Bin Wang,‡[a,b] Qian Liu, [ID][c] Zhenghua Wei,[a,b] Ziye Mou,[d] Quan Li,[a,d] Chunfa Chen, [ID][a,b] Zaichun You,[d] Bang Lin Li, [ID][e] Guansong Wang, [ID] *[a,b] Zhi Xu*[a,b,f] and Hang Qian [ID] *[a,b,f]

Bacterial infection is one of the most serious clinical complications, with life-threatening outcomes. Nature-inspired biomaterials offer appealing microscale and nanoscale architectures that are often hard to fabricate by traditional technologies. Inspired by the light-harvesting nature, we engineered sulfuric acid-treated sunflower sporopollenin exine-derived microcapsules (HSECs) to capture light and bacteria for antimicrobial photothermal therapy. Sulfuric acid-treated HSECs show a greatly enhanced photothermal performance and a strong bacteria-capturing ability against Gram-positive bacteria. This is attributed to the hierarchical micro/nanostructure and surface chemistry alteration of HSECs. To test the potential for clinical application, an *in situ* bacteria-capturing, near-infrared (NIR) light-triggered hydrogel made of HSECs and curdlan is applied in photothermal therapy for infected skin wounds. HSECs and curdlan suspension that spread on bacteria-infected skin wounds of mice first capture the local bacteria and then form hydrogels on the wound upon NIR light stimulation. The combination shows a superior antibacterial efficiency of 98.4% compared to NIR therapy alone and achieved a wound healing ratio of 89.4%. The current study suggests that the bacteria-capturing ability and photothermal properties make HSECs an excellent platform for the phototherapy of bacteria-infected diseases. Future work that can fully take advantage of the hierarchical micro/nanostructure of HSECs for multiple biomedical applications is highly promising and desirable.

Introduction

Bacterial infection and antibiotic resistance have become global challenges in recent years and cost hundreds of millions of dollars each year. The abuse of antibiotics and the rapid development of drug-resistant bacteria call for innovative methods and nanomaterials to combat bacterial infection.[1–4] The skin, as the body's largest organ and the first line of immune defense, plays an important role in repelling external aggression such as bacteria and pathogens.[5] Chronic wounds, such as infected ones, can lead to serious complications, which can be potentially life-threatening.[6] Recently, multifunctional hydrogels have become a promising strategy for infected wound healing.[7–10] Traditional wound dressings, such as bandages and gauze, lack interaction in the process of wound healing and cause secondary wound injury. Owing to the three-dimensional structure, hydrogels have great advantages of a high drug loading capacity and water content, mimicking the extracellular matrix (ECM) and keeping the wound environment moist.[11–13] Curdlan (1,3-β-D-glucan), a carbohydrate polymer, derived from bacteria and fungi has been approved by the FDA as a food additive. The most significant feature of the curdlan biopolymer is its heat-set gelling property.[14,15] Additionally, it has been found to generate inflammatory responses and activate macrophages.[16] Nanoparticles, nanofibers, and curdlan hydrogels have been proven to accelerate wound healing in animal studies.[17–20]

[a]*Institute of Respiratory Diseases, Xinqiao Hospital, Third Military Medical University, 183 Xinqiao Street, Chongqing 400037, China.*
E-mail: hqian@tmmu.edu.cn, wanggs2003@163.com, xu_zhi999@163.com
[b]*Chongqing Key Laboratory of Precision Medicine and Prevention of Major Respiratory Diseases, Chongqing 400037, China*
[c]*Laboratory of Pharmacy and Chemistry, and Laboratory of Tissue and Cell Biology, Lab Teaching & Management Center, Chongqing Medical University, Chongqing 400016, China*
[d]*Department of General Practice, Xinqiao Hospital, Third Military Medical University, Chongqing, 400037, China*
[e]*School of Chemistry and Chemical Engineering, Southwest University, Chongqing 400715, China*
[f]*Yu-Yue Pathology Scientific Research Center, Chongqing, China*
†Electronic supplementary information (ESI) available. See DOI: https://doi.org/10.1039/d3nr04814d
‡These authors contributed equally to this manuscript.

Photothermal therapy (PTT) induced by a near-infrared (NIR) laser has become an effective treatment modality for infected wounds due to its controlled temperature, low toxicity, and non-invasive nature, as well as its ability to accelerate tissue regeneration. It offers an alternative to conventional antibacterial therapy, as it uses NIR light to absorb and convert it into heat to kill bacteria and eradicate biofilms without causing antimicrobial resistance. Various PTT materials, such as organic materials,[21,22] inorganic materials,[23,24] and natural materials,[25–27] have been developed. Generally, PTT agents produce heat and elevate the temperature of a larger area in the local environment, which might cause serious thermal damage to healthy organs and tissues. It is well recognized that engineering the properties of PTT agents to achieve precisely controlled temperatures and to prevent thermal damage to surrounding healthy organs and tissues is desirable.[28] We reasoned that if PTT agents were brought close to pathogens such as bacteria, in a very short distance or even *via* direct contact, in the local environment, the required temperature for PTT would be greatly decreased, thus reducing the thermal damage.

Sunflower sporopollenin exine capsule (SEC) derived hollow microcapsules are a great micro/nano-sized material platform with multiple interesting properties.[29–31] Recently, chemically modified SECs have been shown to be promising microparticles for various research fields due to their strong structure, abundant resource, and good biocompatibility. The robust exine capsule from pollen grains has been used for drug and vaccine delivery in biomedical engineering. Additionally, SEC microparticles have been used as microrobots for killing cancer cells,[32–34] biofilm eradication,[35] optoelectronic applications,[36,37] oil remediation applications,[38] water cleaning, and generating functional multicolor barcodes.[39] Interestingly, several recent studies have found that SECs possess good photothermal properties when exposed to NIR light radiation.[40] However, their photothermal efficiency and

potential for photothermal therapy against bacterial infection, based on SECs, still need to be further explored.

In this study, we constructed HSECs that demonstrated a strong bacteria-capturing capability and significantly improved photothermal efficiency. We further developed a biocompatible, heat-triggered wound dressing that could simultaneously capture bacteria and form multifunctional hydrogels *in situ* based on HSECs. The multifunctional hydrogel was composed of curdlan and HSECs and formed by NIR light irradiation. As illustrated in Scheme 1, HSECs were obtained from natural pollen and treated with sulfuric acid. The protein, esters, and polysaccharide in the spores that may cause immune effects were removed by H_3PO_4 and H_2SO_4.[41] The resultant HSECs were mainly composed of the sporopollenin biopolymer, a safe carbon material. As the nature's most resilient material, sporopollenin exhibits morphological stability under harsh chemical processing, such as acetolysis, acidolysis, and exposure to solvents.[42] Subsequently, employing HSECs as a PTT agent, HSECs and curdlan suspension were injected into the infected wound. The bacteria in the wound were first captured by HSECs in the precursor suspension. Upon NIR light (808 nm) stimulation, the temperature of the precursor suspension increased dramatically, eliminating the bacteria in the infected tissue. Meanwhile, the precursor suspension transformed into HSECs@Curdlan hydrogels *in situ* during the cooling process. Elemental analysis, Fourier Transform Infrared Spectroscopy (FTIR), and Scanning Electron Microscopy (SEM) were employed to characterize the HSECs and HSECs@Curdlan hydrogels. The CLSM and SEM results demonstrated that HSEC hollow microcapsules captured bacteria effectively in between their spikes. HSECs displayed a superior photothermal killing efficiency against *Staphylococcus aureus* (*S. aureus*) under NIR light irradiation *in vitro*. The wound dressing hydrogel HSECs@Curdlan showed excellent antibacterial efficacy and superior biocompatibility *in vivo*. Collectively, this study prepared a natural sunflower pollen-derived microcapsule with an enhanced photothermal performance and developed an

Hang Qian is a professor in Xinqiao Hospital, Third Military Medical University, China. He received his Ph.D. degree from Xiamen University in 2014. During 2014–2016, he worked as a postdoctoral fellow at the Department of Chemical and Biomolecular Engineering, National University of Singapore (NUS), Singapore. His research interests include the design and self-assembly of DNA nanostructures, DNA nanostructure functionalization, and the bioapplications of DNA nanostructures. Currently, he is working on DNA nanostructure-enabled nanomedicines.

Hang Qian
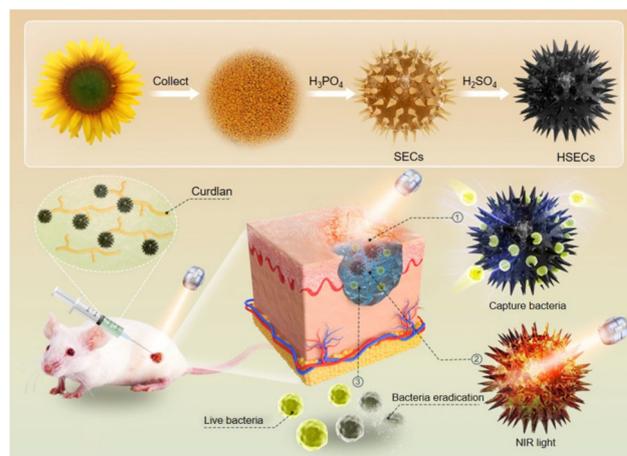
Scheme 1 *In situ* capturing and photothermal sterilization of bacteria accelerate bacteria-infected wound healing.

HSECs@Curdlan hydrogel wound dressing that could *in situ* capture and kill bacteria *in vivo*. The study indicates that the *in situ* capturing concept and light-responsive wound dressings could be a promising strategy for bacteria-infected wound healing in realistic applications.[43–45]

Experimental

Materials

Sunflower pollen was purchased from Jilin province, China. Sulfuric acid (H_2SO_4), hydrochloric acid (HCl), 85% phosphoric acid (H_3PO_4), ethyl ether, acetone, and ethyl alcohol were purchased from Aladdin Biochemical Technology Co., Ltd (Shanghai, China). Curdlan was bought from Macklin Biochemical Technology Co., Ltd (Shanghai, China). LB broth and LB broth agar were obtained from Sangon Biotech Co., Ltd (Shanghai, China).

Preparation of the SECs, HSECs, and HSECs@Curdlan hydrogels

Firstly, 200 mL ethyl ether was mixed with 50 g sunflower pollen and incubated overnight to obtain the defatted pollen. Secondly, 20 g defatted pollen was suspended with 85% phosphoric acid at 70 °C under 300 rpm for 10 h. The suspension was washed with hot water, acetone, HCl (2 M), sterile double distilled water (dd water), acetone, and ethanol and lyophilized in the vacuum freeze dryer to obtain the SECs. Then, 5 g SECs were suspended with 20 mL H_2SO_4 for 15 min and the suspension was washed with a large amount of water and lyophilized in a vacuum freeze dryer to obtain the HSECs. To prepare HSECs@Curdlan hydrogels, 15 mg HSECs and 150 mg curdlan were dissolved in 1 mL dd water and then irradiated with an 808 nm laser for 3 min (2.0 W cm^{-2}).

Characterization

Emission scanning electron microscopy (SEM) and energy-dispersive X-ray spectrometry (EDX) were conducted using a Regulus8100 (Hitachi, Japan) at the accelerating voltage of 2 kV. The SECs, HSECs, and HSECs@Curdlan hydrogels were freeze-dried. Before SEM analysis, the samples were coated with gold to improve their conductivity. Fourier transformation infrared (FTIR) analysis was performed on a VERTEX 80 FTIR spectrometer (Bruker, German). X-ray Photoelectron Spectroscopy (XPS) was conducted using a K-Alpha X-ray photoelectron spectroscopy system (Thermo Fisher Scientific, American). UV-vis spectroscopy was conducted using a UV-Vis-NIR spectrometer UV3600 (Shimadzu Corporation, Japan).

Photothermal properties of SECs, HSECs, HSECs@Curdlan

10 mg SECs and HSECs were exposed to an 808 nm NIR laser for 3 min (1.5 W cm^{-2}). To assess the photothermal properties of Curdlan@HSECs, the suspension containing 15% (W V^{-1}) curdlan and different concentrations of HSECs was irradiated with an 808 nm laser for 3 min (2 W cm^{-2}). To evaluate the differences in the photothermal properties of SECs, HSECs, and HSECs@Curdlan, 15 mg mL^{-1} SECs, HSECs, and HSECs@Curdlan suspension containing 15% (W V^{-1}) curdlan and 15 mg mL^{-1} HSECs were irradiated with an 808 nm laser for 3 min (2 W cm^{-2}). To assess the photostability of HSECs@Curdlan, HSECs@Curdlan containing 15% (W V^{-1}) curdlan and 15 mg mL^{-1} HSECs irradiated with an 808 nm laser for 3 min (2 W cm^{-2}) was recorded in 8 cycles with 3 min laser-on and 2 min laser-off. Real-time photothermal images and temperatures were collected using an FLIR E4 (FLIR Systems Inc, American). The photothermal conversion efficiency (η) was calculated according to the following equation.[46]

$$\eta = [hS\,(T_{max} - T_{surr}) - Q_{dis}]/I\,(1 - 10^{-A808})$$

Bacteria adsorption test

Staphylococcus aureus (*S. aureus*) and *Escherichia coli* (*E. coli*) were cultivated at 37 °C in LB broth overnight. Then, the solution of *S. aureus* and *E. coli* bacteria was centrifuged at 5400g for 2 min and washed with saline twice. The bacteria suspension in saline was diluted to 1×10^9 CFU mL^{-1}. To evaluate the adsorption capacity of HSECs, 15 mg HSECs were added to 1 mL bacterial suspension, respectively. After 30 min co-incubation at 37 °C, to separate the free bacteria and HSECs, the sample was centrifuged at 20g for 3 min. The supernatant was measured using a microplate reader at 600 nm and diluted 100-fold with saline spreading on LB broth agar plates at 37 °C for 12 h, and the samples of bacteria captured by HSECs were collected for confocal laser scanning microscopy (CLSM) and SEM.

In vitro antibacterial experiments

The antibacterial effect of HSECs@Curdlan was determined using the agar diffusion method. 100 μL of the suspension containing HSECs@Curdlan (15% curdlan and different concentrations of HSECs) and *S. aureus* (1×10^7 CFU mL^{-1}) was irradiated with an 808 nm laser for 10 min (2 W cm^{-2}). Real-time photothermal images and temperature were collected using an FLIR E4. After irradiation, 20 μL of the sample was spread on LB broth agar plates incubated at 37 °C for 12 h. The colonies of *S. aureus* on the plate were measured using Image J.

In vitro cytotoxicity assay and hemolysis experiment

To investigate the *in vitro* cytotoxicity of HSECs@Curdlan, the hydrogels (1, 2, 4, 8, 12, 16, 20 mg) were immersed in Roswell Park Memorial Institute (RPMI) 1640 medium (Gibco) supplemented with 10.0% fetal bovine serum (HyClone), 1.0×10^5 U L^{-1} penicillin, and 100.0 mg L^{-1} streptomycin at 37 °C for 24 h and Hacat cells (1×10^4) were seeded in a 96-well plate and cultured for 24 h. After the Hacat cells were incubated for 24 h, the culture media was removed and the hydrogel extract liquid was added into the wells. The cell viability was determined using a CCK8 Kit after 24 h. The LIVE/DEAD cell staining was conducted using an AO/EB staining kit. The blood was obtained from healthy male ICR mice. The blood was centri-

fuged (3000 rpm, 10 min, 4 °C) and washed with saline several times to obtain the red blood cells (RBCs). To prepare the RBC suspension, the RBCs were diluted 20-fold with PBS. After that, 1 mL RBC suspension was incubated with hydrogels at 37 °C for 1 h; dd water and PBS acted as the controls (positive and negative). The samples were incubated at 37 °C for 1 h and centrifuged at 3000 rpm for 10 min to collect the supernatants. These supernatants were measured using a microplate reader with UV-vis spectroscopy at 570 nm. The percent of the hemolysis rate was measured using this equation. Hemolysis (%) = (A sample − A negative)/(A positive − A negative) × 100%.

In vitro immunogenicity assay

BMDMs were extracted from the femur and tibia of C57BL/6 mice (6–8 weeks), and then cultured with macrophage medium containing MaM medium and 100 ng mL^{-1} M-CSF for 6 days.[47] To investigate the in vitro immunogenicity of HSECs@Curdlan, BMDMs were cultured in 6-well plates overnight at a density of 1×10^6 cells per cm^2. Lipopolysaccharide (1 μg mL^{-1}) as a positive control, HSECs (50 μL, 15 mg mL^{-1}), HSECs@Curdlan hydrogel (50 μL, containing 15% curdlan and 15 mg mL^{-1} HSECs) were added and cultured in 1 mL medium for 6 hours. After 6 hours, total RNA was extracted with Trizol reagent and converted to cDNA using the Transcriptor First Strand cDNA Synthesis Kit. Relative expression of the target gene was determined by RT-qPCR using the FastStart Essential DNA Green Master on a Bio-Rad CFX 96 real-time PCR system. The expression value was normalized using GAPDH as an internal control. GAPDH forward: 5′-AGGTCGGTGTGAACGGATTTG-3′, reverse: 5′-GGGGTCGTT GATGGCAACA-3′. TNF-α forward: 5′-GGAACACGTCGTGGGATA ATG-3′, reverse: 5′-GGCAGACTTTGGATGCTTCTT-3′. Interleukin-6 (IL-6) forward: 5′-CTCCCAACAGACCTGTCTATAC-3′, reverse: 5′-CCATTGCACAACTCTTTTCTCA-3′. Interleukin-1β (IL-1β) forward: 5′-TCGCAGCAGCACATCAACAAGAG-3′, reverse: 5′-AGGTCCACGG GAAAGACACAGG-3′.

In vivo animal study

All animal procedures were performed in accordance with the Guidelines for Care and Use of Laboratory Animals of the Third Military Medical University, Laboratory Animal-Guideline for Ethical Review of Animal Welfare (People's Republic of China National Standard GB/T 35892-2018), and approved by the Animal Care and Use Committee of the Third Military Medical University. The mice were anesthetized and the hair on their back was removed. Then, 6 mm diameter full-thickness skin wounds were created by biopsy punch and the suspensions of S. aureus (20 μL, 10^8 CFU mL^{-1}) were directly injected into the wound to establish the S. aureus-infected wound model. After 48 h, these mice were randomly assigned to five groups and received a 50 μL injection of different materials for wound treatment, including Saline, Saline + NIR irradiation (2 W cm^{-2}, 10 min), SECs@Curdlan (containing 15% curdlan and 15 mg mL^{-1} SECs) + NIR irradiation (2 W cm^{-2}, 10 min), HSECs (15 mg mL^{-1} HSECs) + NIR irradiation (2 W cm^{-2}, 10 min), HSECs@Curdlan (containing 15%

curdlan and 15 mg mL^{-1} HSECs) + NIR irradiation (2 W cm^{-2}, 10 min). The wound healing process was monitored using a smartphone for 3 days, and the wound bacteria were collected using cotton swabs for plate counts. The body weights of the mice were measured. After treatment for 9 days, the mice were euthanized, and the wound skin tissue and major organs (heart, liver, spleen, kidneys, and lungs) were isolated for hematoxylin and eosin (H&E) and Masson staining. IL-6 antibodies were used as the marker of inflammatory factors in the wound beds in immunohistochemical staining.

Statistical analysis

All data were expressed as mean ± standard deviation and repeated at least three times. ANOVA analysis and Student's t-test were carried out using GraphPad Prism 8. The level of significance was determined as $p < 0.05$ (*$P < 0.05$, **$P < 0.01$, ***$P < 0.001$).

Results and discussion

Preparation and characterization of HSECs

As shown in Fig. 1A, HSECs were prepared by treating SECs with sulfuric acid for 15 min. After rigorous washing and drying, HSECs were obtained as tan powders. The strong dehydration and carbonization during the sulfuric acid treatment showed the strong oxidizing properties of sulfuric acid. The surface of HSECs is composed of cellulose and lignin, which contain numerous hydroxyl groups that were dehydrated using concentrated sulfuric acid.[48,49] SEM results revealed that HSECs maintained their hollow spherical structures with micrometer-sized spikes and nanopores on their outer surfaces (Fig. 1B). The strong oxidation and dehydration during the sulfuric acid treatment did not disrupt the global structures of HSECs. Energy-dispersive X-ray spectroscopy elemental mapping (EDX) analysis indicated that C, N, and O elements were homogeneously distributed in the HSEC microcapsules (Fig. 1C). X-ray photoelectron spectroscopy (XPS) further confirmed the presence of these elements (Fig. 1D). In addition, the presence of N 1s and S 2p peaks suggested that HSECs might contain sulfur and nitrogen elements. Elementary analysis showed that HSECs were mainly composed of C, H, and O elements, with a small portion of N and S (Table S1†). The bonding status between the different elements in HSECs was further investigated using FTIR (Fig. 1E).

Typical peaks of biomass materials appeared at 1197 cm^{-1}, 1575 cm^{-1}, 1682 cm^{-1}, 2930 cm^{-1}, and 3413 cm^{-1}; indicating the presence of phenolic ring vibration (or C–O–C), aromatic, C=O stretching, out-of-phase CH$_2$ stretching, and O–H stretching, respectively. The SECs had similar chemical groups (Fig. S1†). These results correlated well with the SEC-derived materials reported in other papers.[50] Interestingly, we found that sulfur acid treatment altered the chemical properties of SECs significantly.[41,51] Elementary analysis showed that the contents of N and S were increased from 0.87% and 1.29% to 2.58% and 3.35%, respectively (Table S1†). Generally, sun-
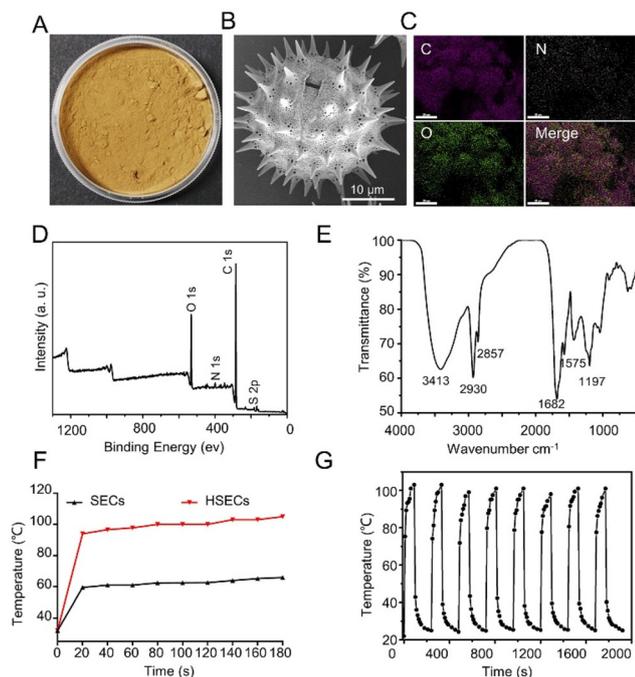
Fig. 1 Preparation and characterization of HSECs. (A) Optical photograph of HSEC powder. (B) SEM image of HSECs. (C) EDX of HSECs, scale bar is 20 μm. (D) XPS spectrum of HSECs. (E) FITR spectrum of HSECs. (F) Temperature elevation curve of HSECs and SEC powders irradiated with 808 nm laser light (1.5 W cm^{-2}) in the solid state. (G) Temperature profiles of HSECs for 8 cycles of on–off laser irradiation (1.5 W cm^{-2}, 808 nm).

flower pollen grains were initially treated with H_3PO_4 to remove the proteins and biomass inside the microcapsules. In this study, we purposely treated SECs with sulfur acids to further modify their chemical properties. The peak at 1197 cm^{-1} (C–O–C) of the HSECs was enhanced compared to the SECs, along with an increase in the intensity of the O 1s orbitals, both of which could contribute to the dehydration reaction of the SECs' hydroxyl groups (Fig. S2†). We believe that the significant enhancement of the peak at 1680 cm^{-1} (C=O stretching) in the HSECs is a result of the oxidization reaction caused by sulfuric acid treatment of the SECs. Additionally, the peak at 1575 cm^{-1} (aromatic) also increased, indicating that some of the lignins are exposed outside of the HSEC layer. Consequently, the macroscopic chemical composition of HSECs was remarkably changed, which could benefit their potential biomedical application.

We next evaluated the photothermal properties of HSEC powder. After irradiation with NIR light for 3 min, a significant increase in temperature (increased by 73 °C) was observed for HSECs (Fig. 1F). In contrast, the temperature of SECs only increased by 33 °C. The photothermal performances of HSECs were tested for multiple circles of on–off laser irradiation.

Temperature profiles indicated that HSECs exhibited robust and stable photothermal efficiencies up to 8 cycles (Fig. 1G). Additionally, the photothermal efficiencies of HSECs and SECs were evaluated to be 7.1% and 4.1%, respectively. These

results suggested that HSECs had better photothermal efficiency than SECs. Additionally, we measured the photothermal conversion efficiency of HSECs under different laser intensities. The photothermal efficiency of HSECs increases with the power of laser illumination, reaching 3.5% at 1.5 W cm^{-2} and 12.7% at 2.5 W cm^{-2} (Fig. S3†). Previously, we had found that SECs extracted from sunflower pollen displayed good photothermal efficiency. The origin of photothermal properties could likely be attributed to the presence of a unique spike structure and the surface chemical groups of the SECs, as suggested by other groups.[40] The FTIR curve of HSECs (Fig. 1D) appeared at 1575 cm^{-1}, 1682 cm^{-1} and 3413 cm^{-1}, which were assignable to aromatic and carbonyl groups and hydroxyl groups, indicating the presence of lignin.[52] Lignin is a type of aromatic biopolymer that allows for the formation of strong conjugation and π–π molecular interactions among lignin molecules.[53] We speculate that the existence of lignin and the special structure of HSECs are responsible for the photothermal efficiency. In the current study, we improved the photothermal performances of SECs considerably through chemical processing with sulfuric acid. The improved photothermal properties might be attributed to the chemical property changes introduced by sulfuric acid. For example, compared with SECs, the intensity of O 1s orbitals was significantly increased for HSECs (Fig. S2†). UV-Vis-NIR spectrum of HSECs and SECs showed that HSECs had stronger absorbance than SECs at around 808 nm. The absorbances of HSECs and SECs at 808 nm were 0.35 and 0.13, respectively (Fig. S4†). However, the detailed underlying mechanisms need to be investigated further.

HSECs capture bacteria *in vitro*

Inspired by the hierarchical structures of HSECs, we explored the bacteria-capturing ability of HSECs *in vitro*. Gram-positive *S. aureus* and Gram-negative *E. coli* were selected to evaluate HSECs' capturing efficiency. As shown in Fig. 2A, HSECs were first mixed with bacteria for 30 min, and the quantity of bacteria in the supernatant was measured by the spread plate count method. HSECs were collected to examine the bacteria-capturing ability by SEM. The colonies plate of the supernatant of HSECs with *S. aureus* displayed fewer bacteria colonies (Fig. 2B right) compared to the untreated group (Fig. 2B left), indicating that some of the *S. aureus* in the mixture may have been captured by HSECs. Similarly, we observed bacteria-capturing phenomena for the Gram-negative bacteria *E. coli* (Fig. 2C). Notably, HSECs had a much better capturing efficiency for *S. aureus* than for *E. coli*. CLSM imaging showed that a considerable amount of spherical *S. aureus* was captured on the spiky surface of HSECs. The spherical structure indicated by the red arrow in the left panel of the image is *S. aureus*. (Fig. 2D). The most convincing evidence of the bacteria-capturing ability of HSECs came from SEM (Fig. 2E). The zoom-in image in the right panel of Fig. 2E clearly showed the spherical *S. aureus* located around the spikes of HSECs. Similarly, we observed the same bacteria-capturing phenomena for the Gram-negative bacteria *E. coli* (Fig. 2F and G).
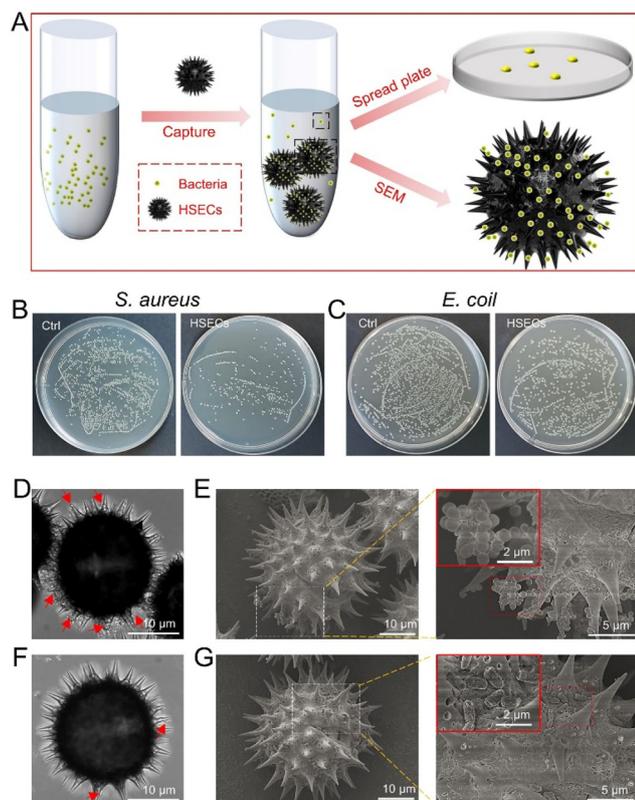
Fig. 2 HSECs capture bacteria *in vitro*. (A) Schematic of diagram of the bacteria captured by HSECs. (B) Photographs of *S. aureus* colony plates of the HSECs/*S. aureus* mixture supernatant. (C) Photographs of *E. coli* colony plates of the HSECs/*E. coli* supernatant. (D) The confocal image shows a bright field of *S. aureus* captured by HSECs. (E) SEM image of *S. aureus* captured by HSECs. (F) The confocal image shows a bright field of *E. coli* captured by HSECs. (G) SEM images of *E. coli* captured by HSECs.

However, the absorption of *E. coli* by HSECs appeared much less efficient than that of *S. aureus*. We then measured the optical density (OD) values of the supernatant after bacteria absorption at 600 nm to quantify the residues of bacteria left in the suspension by centrifuging down the HSECs. Semi-quantitative analysis indicated that the capturing efficiencies for *S. aureus* and *E. coli* were 76.6% and 32.5%, respectively, in the current experimental settings (Fig. S5†). A few previous reports have shown that rough surfaces can facilitate the absorption of bacteria.[54–60] It is hypothesized that the absorption ability of rough surfaces may be due to physical interactions such as structural entangling. Indeed, SECs have some bacterial adsorption capacity but are much less efficient than HSECs in adsorbing *Staphylococcus aureus*. (Fig. S5†). Therefore, we reckoned that the greater bacteria-capturing ability of HSECs may not only stem from the spiky morphology but also from potential physical adsorption with the HSEC surface. Physical adsorption is a straightforward method in which HSECs attach to *S. aureus* through various interactions, such as topological interactions, hydrogen bonding, and intermolecular π–π-stacking.[56,58,60,61] The rough surface of HSECs

and the hairy structure of bacteria contribute to the topological interactions. Additionally, hydrogen bonding occurs between the hydroxyl groups of HSECs and the cell wall of *S. aureus*. Furthermore, the functional groups of aromatic and carbonyl groups of HSECs enable intermolecular π–π-stacking, further enhancing the ability of bacterial adsorption. Notably, the increase of sulfur and nitrogen contents in HSECs, as well as the significant increase of O 1s intensity from XPS spectra, may play certain roles in the bacteria absorption enhancement. Nevertheless, the detailed interaction mechanisms between HSECs and bacteria still require further investigation.

HSECs@Curdlan hydrogel formation and photothermal evaluation

Due to the excellent photothermal efficiency and bacteria-capturing properties, HSECs were employed to design a temperature-sensitive hydrogel, HSECs@Curdlan. Curdlan is a neutral homopolysaccharide and its suspension can form a hydrogel by heating at a temperature above 55 °C followed by cooling. The HSECs@Curdlan suspension was a brown solution (Fig. 3A, left and middle), which after being irradiated with NIR light for 3 min (2 W cm^{-2}) followed by cooling, was shown to form a gel (Fig. 3A, right). This was further confirmed by SEM, which revealed the hydrogel's 3D internal porous structure with HSECs dispersed on both its surface and intracellular space (Fig. 3B), and the porosity rate is approximately 46.8% (Fig. S6†). In addition, the compressive strength of the HSECs@Curdlan is 40.87 MPa (Fig. S7†). To assess the photothermal efficiency of HSECs@Curdlan for photothermal therapy, the temperature-change tendencies of HSECs@Curdlan suspensions with different concentrations of HSECs were measured under NIR light irradiation. Fig. 3C and D demonstrate how the temperature rises rapidly within 60 s and reaches a plateau at HSEC concentrations of over 1 mg mL^{-1}. Furthermore, the highest temperature increase of 33.2 °C was recorded for the 20 mg mL^{-1} HSEC concentration. In contrast, the temperatures of blank curdlan and 1 mg mL^{-1} HSEC groups had negligible increases. Therefore, HSECs@Curdlan containing 15 mg mL^{-1} HSECs was selected for further experiments. Fig. 3E compares the photothermal performances of SECs, HSECs, and HSECs@Curdlan in the liquid phase. At the 60 s time point, while the temperatures of HSECs and HSECs@Curdlan had risen 25.3 °C and 26.0 °C respectively, the SECs suspension had only increased by 6.1 °C, demonstrating that the photothermal efficiency of HSECs was superior to that of SECs in the liquid phase and that the addition of Curdlan had no notable impact on the photothermal efficiency of HSECs. Lastly, to test the reusability of HSECs@Curdlan, 8 cycles of temperature rising and lowering of the same under NIR light irradiation were recorded. As shown in Fig. 3F, no obvious temperature decrease was observed in each cycle.

Antibacterial activity of HSECs@Curdlan *in vitro*

Given the excellent photothermal efficiency and bacteria-capturing efficiency of HSECs and HSECs@Curdlan, the antibac-
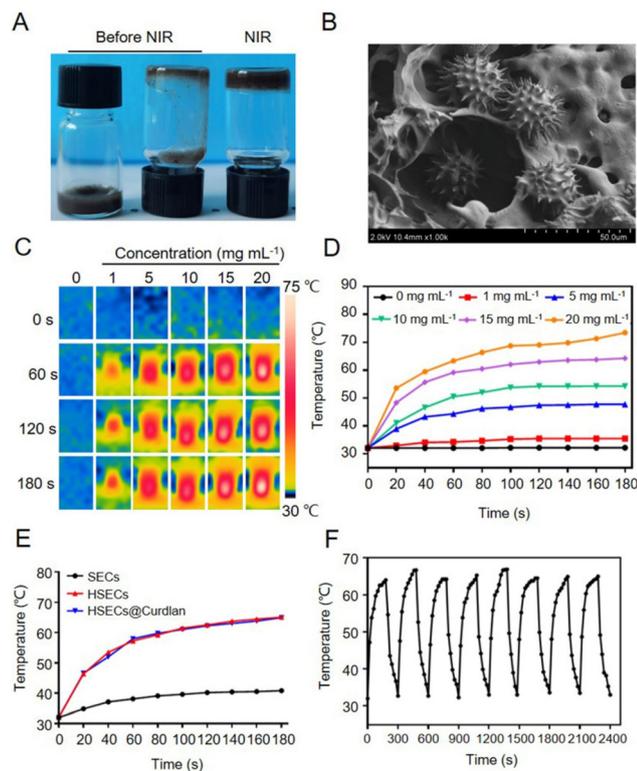
Fig. 3 Preparation, characterization, and photothermal evaluation of HSECs@Curdlan. (A) Photograph of the HSECs@Curdlan hydrogel before (left and middle) and after (right) 808 nm laser irradiation. (B) SEM images of the HSECs@Curdlan hydrogel. Photothermal images (C) and (D) heating curves of different concentrations of the HSECs@Curdlan solution under 808 nm irradiation (2.0 W cm^{-2}). (E) Temperature curves of 15 mg mL^{-1} SECs, 15 mg mL^{-1} HSECs, and HSECs@Curdlan (containing 15 mg mL^{-1} HSECs) at different time points under 808 nm light irradiation (2.0 W cm^{-2}). (F) Temperature profiles of HSECs@Curdlan (containing 15 mg mL^{-1} HSECs) for 8 cycles of on−off laser irradiation (2.0 W cm^{-2}, 808 nm).

Fig. 4 NIR light-driven antibacterial effects of HSECs@Curdlan against *S. aureus*. (A) Bacterial survival rates of *S. aureus* treated with HSECs@Curdlan containing different concentrations of HSECs with and without 808 nm (2.0 W cm^{-2}, 10 min) light irradiation ($n = 3$, *$P < 0.05$, ***$P < 0.001$). (B) Temperature elevation of the HSECs@Curdlan and *S. aureus* mixture containing different concentrations of HSECs under 808 nm 2.0 W cm^{-2} irradiation for 10 min. (C) Representative photographs of *S. aureus* colony plates after being treated with HSECs@Curdlan containing different concentrations of HSECs.

terial performance of HSECs@Curdlan was measured by the spread-plate count method. Gram-positive *S. aureus* (1 × 10⁷ CFU mL^{-1}) was incubated with HSECs@Curdlan containing a HSEC concentration ranging from 0 to 20 mg mL^{-1} and irradiated with NIR light for 10 min. As illustrated in Fig. 4A, there was no obvious antibacterial effect of HSECs@Curdlan without NIR irradiation. After irradiation, the antibacterial effects increased with higher HSEC concentrations in HSECs@Curdlan. Notably, HSECs@Curdlan with concentrations higher than 5 mg mL^{-1} showed a significant killing effect against *S. aureus*. When the concentration of HSECs was higher than 10 mg mL^{-1}, the antibacterial survival rate of the HSECs@Curdlan-treated group was only 0.1%. These results suggested that HSECs@Curdlan exhibited excellent antibacterial effects *in vitro*. Fig. 4B showed the photothermal performances of HSECs@Curdlan with different HSEC concentrations in the presence of *S. aureus*. As expected, HSECs@Curdlan showed similar temperature profiles, as indicated in Fig. 3D. Spread plate count assay results further confirmed the photothermal killing effects of HSECs@Curdlan (Fig. 4C).
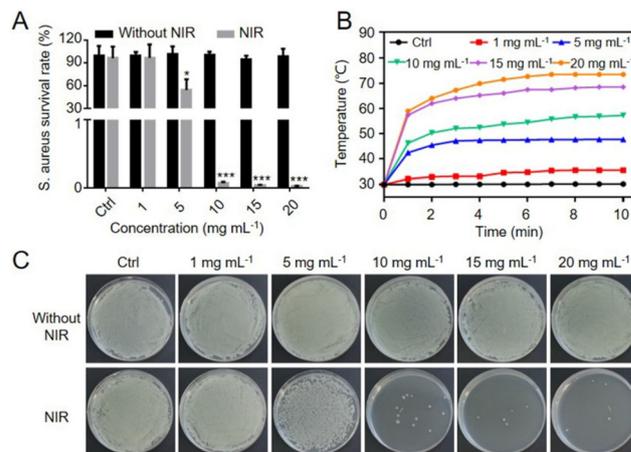
HSECs@Curdlan exhibited relatively lower bacterial-killing efficiency for *E. coli* than for *S. aureus* at 10 mg mL^{-1} (Fig. S8†). In line with the survival rate data in Fig. 4A, *S. aureus* colonies were significantly reduced when the HSEC concentration in HSECs@Curdlan was higher than 10 mg mL^{-1}.

Biosafety of HSECs@Curdlan

The biocompatibility of the HSECs@Curdlan hydrogel was critical for biomedical applications. As shown in Fig. 5A, the hemolysis ratio of HSECs@Curdlan hydrogels of different concentrations was all lower than 5%. To test the cytocompatibility of the hydrogel, Hacat cells were exposed to different concentrations of HSECs@Curdlan hydrogels immersed in the medium culture for 24 h and tested by the CCK8 assay. As shown in Fig. 5B, HSECs@Curdlan showed no cytotoxicity to cells up to a concentration of 20 mg mL^{-1}.

Additionally, a Cell Live/Dead Kit was used to directly observe the cell viability, which revealed *via* fluorescence imaging that most of the cells were alive (Fig. 5C). To evaluate the immunogenicity of HSECs@Curdlan *in vitro*, BMDM cells were cultured with HSECs and HSECs@Curdlan hydrogel. LPS-challenged BMDMs were applied as a positive control. We examined the inflammatory factors after culturing the cells with the materials using RT-qPCR. The mRNA expression levels of TNF-α, IL-6, and IL-1β of HSECs and HSECs@Curdlan were significantly lower than those in the LPS group, showing a mild inflammatory response (Fig. S9†). These results suggested that the HSECs@Curdlan hydrogel has excellent cytocompatibility and hemocompatibility, and is safe for wound healing applications.
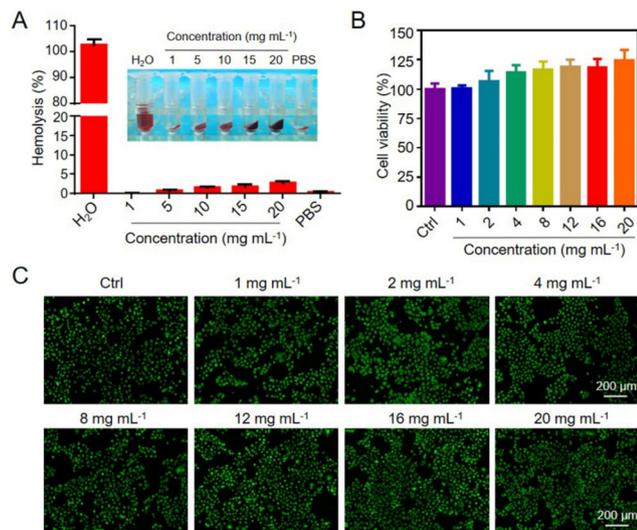
Fig. 5 Hemolysis assessment and cytotoxicity for the HSECs@Curdlan hydrogel. (A) Photographs and count of the hemolytic ratio of the HSECs@Curdlan hydrogel dispersion at different concentrations. (B) Cell viability and (C) live/dead test of the HSECs@Curdlan hydrogel dispersion at different concentrations.

HSECs@Curdlan accelerates bacteria-infected wound healing *in vivo*

To investigate the photothermal sterilization ability of HSECs@Curdlan *in vivo*, we built an *S. aureus*-infected mouse wound model (Fig. 6A). In brief, 6 mm skin wounds were created and infected with *S. aureus*. After two days, HSECs@Curdlan was prepared and spread onto the wound for the evaluation of *in vivo* wound healing. For comparison, five groups were applied: Saline, Saline + NIR, SECs@Curdlan + NIR, HSECs + NIR, and HSECs@Curdlan + NIR. As shown in Fig. 6B, the temperatures of the wound region for the HSECs + NIR and HSECs@Curdlan + NIR groups increased from 28.8 °C to 56.5 °C and from 29.0 °C to 56.0 °C, respectively. In contrast, the temperatures of the Saline + NIR and SECs@Curdlan + NIR groups only increased by 1.3 °C and 7.0 °C, respectively. This result shows that HSECs@Curdlan indeed have better photothermal efficiency than SECs@Curdlan *in vivo*. Notably, the temperature increases between HSECs and HSECs@Curdlan were very close, implying that the addition of curdlan didn't significantly alter the photothermal performances. Additionally, the temperature profiles of the four groups under NIR light stimulation are presented in Fig. 6C. Due to the thermal sensitivity of curdlan, the HSECs@Curdlan hydrogel was able to perfectly coat the wound after NIR light irradiation. Moreover, the *in situ* formation of the HSECs@Curdlan hydrogel on the wound could be observed as shown in Fig. S10.† The HSECs in the HSECs@Curdlan captured and concentrated the local bacteria which in turn facilitated the photothermal sterilization. Furthermore, the *in situ*-created HSECs@Curdlan hydrogels provided a micro-
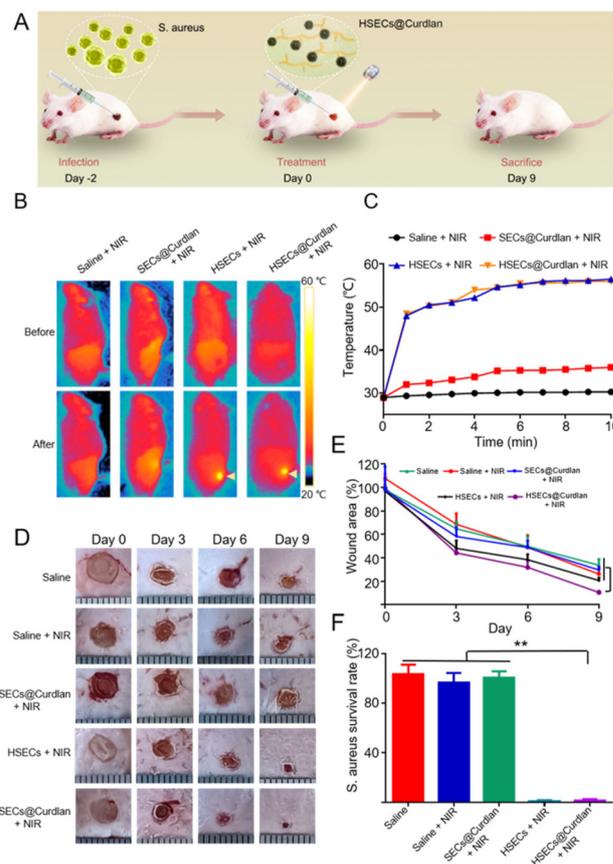

Fig. 6 (A) Schematic illustration of the photothermal therapy for *S. aureus*-infected wounds *in vivo*. (B) Photothermal images and (C) temperature elevation of each group of treated wounds upon 808 nm laser irradiation (2.0 W cm^{-2}, 10 min). (D) Photographs of mice wounds from day 0 to 9. (E) Wound closure evolution from day 0 to 9 (two way-ANOVA, $n = 3$,**$P < 0.01$). (F) Quantitative analysis of *S. aureus* on wounds (one way-ANOVA, $n = 3$, **$P < 0.01$).

environment for cell proliferation and expedited wound skin regeneration. With the formation of a scar, the hydrogel on the wound area fell off along with the scar at the end of the *in vivo* experiment (Fig. S10†). The images of the wound area were monitored using a smartphone on day 0, 3, 6, and 9 (Fig. 6D). Out of all groups, the HSECs@Curdlan + NIR group exhibited the most remarkable healing effect on day 9, where the infected wound area achieved a healing ratio of about 89.4%. The wound area of the HSECs + NIR group achieved a healing ratio of about 80.2%, while the SECs@Curdlan + NIR group, Saline + NIR group, and Saline group only achieved a healing ratio of about 71.3%, 66.3% and 73.7%, respectively (Fig. 6E).

Quantitative analysis showed that the average wound area of HSECs@Curdlan + NIR treated groups was much lesser than that of Saline, Saline + NIR, and SECs@Curdlan + NIR groups throughout all treatment periods (Fig. 6E). A spread plate count method was utilized on day 3 to check the antibacterial capability of HSECs@Curdlan (Fig. S11†). Among all groups, the HSECs + NIR group and HSECs@Curdlan + NIR

group had slight *S. aureus* colonies present while the other groups showed great numbers of bacteria colonies. Quantitative analysis demonstrated that bacteria of the HSECs@Curdlan + NIR treated group was almost totally eradicated (Fig. 6F). These results indicated that the photothermal therapy of HSECs@Curdlan was effective and HSECs@Curdlan could enhance wound healing. The body weight of all groups was examined during the *in vivo* validation and no prominent differences were observed among all groups (Fig. S12†). H&E staining of the primary organs (heart, liver, spleen, lungs, and kidneys) revealed that no detectable damages were seen after 9 days of treatment, demonstrating the great biosafety of HSECs@Curdlan (Fig. S12†). H&E and Masson staining were employed in a skin section analysis to further inspect the healing effects of HSECs@Curdlan with NIR light. As seen in Fig. 7, the HSECs@Curdlan + NIR group displayed a much smaller granulation tissue gap compared to the other groups, suggesting that HSECs@Curdlan + NIR treatment-initiated skin tissue regeneration. Additionally, H&E staining images showed that numerous inflammatory cells (represented by red arrows) were present in the Saline group, Saline + NIR group, and SECs@Curdlan + NIR group, while the HSECs@Curdlan + NIR group indicated considerably lesser amounts. This implies that HSECs@Curdlan + NIR treatment more effectively reduces the inflammatory responses. Masson's trichrome staining showed that in the healed area of the wounds, the collagen arrangement in the HSECs@Curdlan + NIR group-treated wounds was more complete compared to the other groups (Fig. 7). Meanwhile, the expression of interleukin (IL-6) at the wound site was assessed by an immunohistochemistry assay to evaluate HSECs' inflammatory response. As shown in Fig. S13,† the Saline group, Saline + NIR group, and SECs@Curdlan + NIR group exhibited a higher level of IL-6 on day 9, while the HSECs + NIR group and HSECs@Curdlan + NIR group showed a mild inflammation, which is consistent with the results of wound healing shown in Fig. 7. These results indicated that HSECs@Curdlan with NIR light irradiation could destroy bacteria and stimulate wound regeneration *in vivo*.
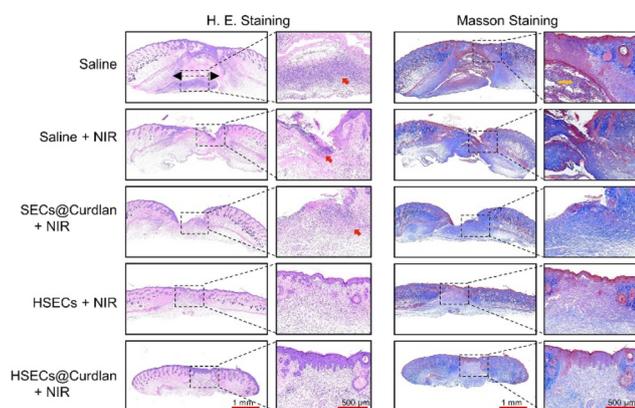

Fig. 7 H&E Staining and Masson staining of mice wounds at day 9.

Conclusions

In summary, natural sunflower pollen grain-derived microcapsules called HSECs were developed with superior bacterial adsorption and photothermal efficiency. HSECs were further used to create an *in situ* bacterial capturing and light-responsive HSECs@Curdlan hydrogel wound dressing which was applied to bacteria-infected wound healing *in vivo*. The SEM and CLSM imaging results confirmed the rapid capture of bacteria on the hierarchical surface of the HSECs, especially for Gram-positive bacteria *S. aureus*. Hemolysis assessment and cell viability assays showed that the HSECs@Curdlan microcapsules were safe and non-toxic. When employed both *in vitro* and *in vivo*, HSECs@Curdlan and the accompanying NIR light irradiation were able to effectively eliminate *S. aureus*, promoting wound healing. This strategy of *in situ* capturing and killing could be useful for other skin disease therapies, and we anticipate that the hierarchical structure and surface properties of HSEC microcapsules can continue to be modified for various biomedical applications.

Author contributions

Yao Yang: investigation, formal analysis, methodology, and writing. Bin Wang: methodology, investigation, writing, and funding acquisition. Qian Liu: investigation and writing – review & editing. Zhenghua Wei: investigation and supervision. Ziye Mou: Investigation and formal analysis. Quan Li: investigation. Chunfa Chen: investigation. Zaichun You: investigation. Banglin Li: writing and supervision. Guansong Wang: conceptualization, supervision, and review & editing. Zhi Xu: conceptualization, supervision, and funding acquisition. Hang Qian: conceptualization, supervision, writing – review & editing, and funding acquisition.

Conflicts of interest

There are no conflicts to declare.

Acknowledgements

References

1 K. Zheng and J. Xie, Composition-Dependent Antimicrobial Ability of Full-Spectrum AuxAg25-x Alloy Nanoclusters, *ACS Nano*, 2020, **14**, 11533.

2 B. L. Li, J. J. Luo, H. L. Zou, Q.-M. Zhang, L.-B. Zhao, H. Qian, H. Q. Luo, D. T. Leong and N. B. Li, Chiral nano-crystals grown from MoS2 nanosheets enable photother-mally modulated enantioselective release of antimicrobial drugs, *Nat. Commun.*, 2022, **13**(1), 7289.

3 K. Zheng and J. Xie, Engineering Ultrasmall Metal Nanoclusters as Promising Theranostic Agents, *Trends Chem.*, 2020, **5**, 1844.

4 K. Zheng, M. I. Setyawati, D. T. Leong and J. Xie, Antimicrobial silver nanomaterials, *Coord. Chem. Rev.*, 2018, **357**, 1.

5 R. Li, K. Liu, X. Huang, D. Li, J. Ding, B. Liu and X. Chen, Bioactive Materials Promote Wound Healing through Modulation of Cell Behaviors, *Adv. Sci.*, 2022, **9**, 2105152.

6 F. Huang, X. Lu, Y. Yang, Y. Yang, Y. Li, L. Kuai, B. Li, H. Dong and J. Shi, Microenvironment-Based Diabetic Foot Ulcer Nanomedicine, *Adv. Sci.*, 2022, **10**, 2203308.

7 M. Kharaziha, A. Baidya and N. Annabi, Rational Design of Immunomodulatory Hydrogels for Chronic Wound Healing, *Adv. Mater.*, 2021, **33**, 2100176.

8 Y. Xu, H. Chen, Y. Fang and J. Wu, Hydrogel Combined with Phototherapy in Wound Healing, *Adv. Healthcare Mater.*, 2022, **11**, 2200494.

9 H. Yao, M. Wu, L. Lin, Z. Wu, M. Bae, S. Park, S. Wang, W. Zhang, J. Gao, D. Wang and Y. Piao, Design strategies for adhesive hydrogels with natural antibacterial agents as wound dressings: Status and trends, *Mater. Today Bio*, 2022, **16**, 100429.

10 D. Stern and H. Cui, Crafting Polymeric and Peptidic Hydrogels for Improved Wound Healing, *Adv. Healthcare Mater.*, 2019, **8**, 1900104.

11 N. Mohammad Hadi, P.-G. Sara Cristina, S.-S. Mónica Gabriela, Á. Mario Moisés and S. Grissel Trujillo de, Structural and biological engineering of 3D hydrogels for wound healing, *Bioact. Mater.*, 2022, **24**, 197.

12 A. Maleki, J. He, S. Bochani, V. Nosrati, M.-A. Shahbazi and B. Guo, Multifunctional Photoactive Hydrogels for Wound Healing Acceleration, *ACS Nano*, 2021, **15**, 18895.

13 L. P. da Silva, R. L. Reis, V. M. Correlo and A. P. Marques, Hydrogel-Based Strategies to Advance Therapies for Chronic Skin Wounds, *Annu. Rev. Biomed. Eng.*, 2019, **21**, 145.

14 D. K. Verma, A. K. Niamah, A. R. Patel, M. Thakur, K. Singh Sandhu, M. L. Chávez-González, N. Shah and C. Noe Aguilar, Chemistry and microbial sources of curdlan with potential application and safety regulations as prebiotic in food and health, *Food Res. Int.*, 2020, **133**, 109136.

15 R. Zhang and K. J. Edgar, Properties, Chemistry, and Applications of the Bioactive Polysaccharide Curdlan, *Biomacromolecules*, 2014, **15**, 1079.

16 G. D. Brown and S. Gordon, Immune recognition. A new receptor for beta-glucans, *Nature*, 2001, **413**(6851), 36.

17 L. M. van den Berg, E. M. Zijlstra-Willems, C. D. Richters, M. M. W. Ulrich and T. B. H. Geijtenbeek, Dectin-1 acti-vation induces proliferation and migration of human kera-tinocytes enhancing wound re-epithelialization, *Cell. Immunol.*, 2014, **289**, 49.

18 R. Yunus Basha, T. S. Sampath Kumar, R. Selvaraj and M. Doble, Silver Loaded Nanofibrous Curdlan Mat for Diabetic Wound Healing: An In Vitro and In Vivo Study, *Macromol. Mater. Eng.*, 2018, **303**, 1800234.

19 M. Lin, H. Long, M. Liang, B. Chu, Z. Ren, P. Zhou, C. Wu, Z. Liu and Y. Wang, Antifracture, Antibacterial, and Anti-inflammatory Hydrogels Consisting of Silver-Embedded Curdlan Nanofibrils, *ACS Appl. Mater. Interfaces*, 2021, **13**, 36747.

20 T. Ganbold and H. Baigude, Design of Mannose-Functionalized Curdlan Nanoparticles for Macrophage-Targeted siRNA Delivery, *ACS Appl. Mater. Interfaces*, 2018, **10**, 14463.

21 H. Wang, J. Chang, M. Shi, W. Pan, N. Li and B. Tang, A Dual-Targeted Organic Photothermal Agent for Enhanced Photothermal Therapy, *Angew. Chem., Int. Ed.*, 2018, **58**, 1057.

22 H. S. Jung, P. Verwilst, A. Sharma, J. Shin, J. L. Sessler and J. S. Kim, Organic molecule-based photothermal agents: an expanding photothermal therapy universe†, *Chem. Soc. Rev.*, 2018, **47**, 2280.

23 P. Tang, Y. Liu, Y. Liu, H. Meng, Z. Liu, K. Li and D. Wu, Thermochromism-induced temperature self-regulation and alternating photothermal nanohelix clusters for synergistic tumor chemo/photothermal therapy, *Biomaterials*, 2018, **188**, 12.

24 Z. Jiang, C. Zhang, X. Wang, M. Yan, Z. Ling, Y. Chen and Z. Liu, A Borondifluoride-Complex-Based Photothermal Agent with an 80% Photothermal Conversion Efficiency for Photothermal Therapy in the NIR-II Window, *Angew. Chem., Int. Ed.*, 2021, **60**, 23376.

25 M. A. Kim, S. D. Yoon, E.-M. Kim, H.-J. Jeong and C.-M. Lee, Natural melanin-loaded nanovesicles for near-infrared mediated tumor ablation by photothermal conver-sion, *Nanotechnology*, 2018, **29**, 415101.

26 Y. Liu, L. Zhao, G. Shen, R. Chang, Y. Zhang and X. Yan, Coordination self-assembly of natural flavonoids into robust nanoparticles for enhanced in vitro chemo and photothermal cancer therapy, *Colloids Surf., A*, 2020, **598**, 124805.

27 X. Wang, X. Liu, Z. Ma, C. Mu and W. Li, Photochromic and photothermal hydrogels derived from natural amino acids and heteropoly acids, *Soft Matter*, 2021, **17**, 10140.

28 J. Wang, B. Hao, K. Xue, H. Fu, M. Xiao, Y. Zhang, L. Shi and C. Zhu, A Smart Photothermal Nanosystem with an Intrinsic Temperature-Control Mechanism for Thermostatic Treatment of Bacterial Infections, *Adv. Mater.*, 2022, **24**, 2205653.

29 A. Radja, E. M. Horsley, M. O. Lavrentovich and A. M. Sweeney, Pollen Cell Wall Patterns Form from Modulated Phases, *Cell*, 2019, **176**, 856.

30 T.-F. Fan, S. Park, Q. Shi, X. Zhang, Q. Liu, Y. Song, H. Chin, M. S. B. Ibrahim, N. Mokrzecka, Y. Yang, H. Li, J. Song, S. Suresh and N.-J. Cho, Transformation of hard pollen into soft matter, *Nat. Commun.*, 2020, **11**, 1449.

31 M. G. Potroz, R. C. Mundargi, J. J. Gillissen, E.-L. Tan, S. Meker, J. H. Park, H. Jung, S. Park, D. Cho, S.-I. Bang and N.-J. Cho, Plant–Based Hollow Microcapsules for Oral Delivery Applications: Toward Optimized Loading and Controlled Release, *Adv. Funct. Mater.*, 2017, **27**, 1700270.

32 S. Xin, Y. Yunru, W. Dan, W. Fang, S. Weijian, D. Ping and S. Luoran, Spiny pollen-based antigen-presenting clusters for promoting T cells expansion, *Chem. Eng. J.*, 2022, **437**, 135374.

33 C. C. Mayorga-Martinez, M. Fojtů, J. Vyskočil, N. J. Cho and M. Pumera, Pollen-Based Magnetic Microrobots are Mediated by Electrostatic Forces to Attract, Manipulate, and Kill Cancer Cells, *Adv. Funct. Mater.*, 2022, **32**, 1700270.

34 M. J. Uddin and H. S. Gill, Ragweed pollen as an oral vaccine delivery system: Mechanistic insights, *J. Controlled Release*, 2017, **268**, 146.

35 M. Sun, K. F. Chan, Z. Zhang, L. Wang, Q. Wang, S. Yang, S. M. Chan, P. W. Y. Chiu, J. J. Y. Sung and L. Zhang, Magnetic Microswarm and Fluoroscopy-Guided Platform for Biofilm Eradication in Biliary Stents, *Adv. Mater.*, 2022, **34**, 2201888.

36 Y. Hwang, A. Sadhu, S. Shin, S. W. Leow, Z. Zhao, J. Deng, J. A. Jackman, M. Kim, L. H. Wong and N.-J. Cho, An Intrinsically Micro-/Nanostructured Pollen Substrate with Tunable Optical Properties for Optoelectronic Applications, *Adv. Mater.*, 2021, **33**, 2100566.

37 D. Xia, Q. Chen, Y. Jiao, Q. Lian, M. Sun, C. He, J. Shang and T. Wang, A modified flower pollen-based photothermo-catalytic process for enhanced solar water disinfection: Photoelectric effect and bactericidal mechanisms, *Water Res.*, 2022, **217**, 118423.

38 Y. Hwang, M. S. B. Ibrahim, J. Deng, J. A. Jackman and N. J. Cho, Colloid-Mediated Fabrication of a 3D Pollen Sponge for Oil Remediation Applications, *Adv. Funct. Mater.*, 2021, **31**, 2101091.

39 Y. Wang, Y. Wang, F. Bian, L. Shang, Y. Shu and Y. Zhao, Quantum Dots Integrated Biomass Pollens as Functional Multicolor Barcodes, *Chem. Eng. J.*, 2020, **395**, 125106.

40 Y. Yang, Q. Zhang, J. Zhang, A. Chen, Y. Chen, S. Li, M. Ye, X. Xuan, X. Li, H. He and J. Wu, Natural pollen extract for photothermal therapy, *Mater. Des.*, 2021, **202**, 109573.

41 R. C. Mundargi, M. G. Potroz, S. Park, H. Shirahama, J. H. Lee, J. Seo and N.-J. Cho, Natural Sunflower Pollen as a Drug Delivery Vehicle, *Small*, 2015, **12**, 1167.

42 P. Guzmán-Delgado and M. A. Zwieniecki, The makeup of a gamete space capsule, *Nat. Plants*, 2019, **5**, 8.

43 M. Aono, Y. Bando and K. Ariga, Nanoarchitectonics: pioneering a new paradigm for nanotechnology in materials development, *Adv. Mater.*, 2012, **24**, 150.

44 K. Ariga and J. Li, Nanoarchitectonics for Advanced Materials: Strategy Beyond Nanotechnology, *Adv. Mater.*, 2016, **28**, 987.

45 W. Chaikittisilp, Y. Yamauchi and K. Ariga, Material Evolution with Nanotechnology, Nanoarchitectonics, and Materials Informatics: What will be the Next Paradigm Shift in Nanoporous Materials, *Adv. Mater.*, 2021, **34**, 2107212.

46 D. K. Roper, W. Ahn and M. Hoepfner, Microscale Heat Transfer Transduced by Surface Plasmon Resonant Gold Nanoparticles, *J. Phys. Chem. C*, 2007, **111**, 3636–3641.

47 I. Pineda-Torra, M. Gage, A. de Juan and O. M. Pello, Isolation, Culture, and Polarization of Murine Bone Marrow-Derived and Peritoneal Macrophages, *Methods Mol. Biol.*, 2015, **1339**, 101.

48 F. Björnerbäck and N. Hedin, Microporous Humins Prepared from Sugars and Bio-Based Polymers in Concentrated Sulfuric Acid, *ACS Sustainable Chem. Eng.*, 2019, **7**, 1018–1027.

49 C. Wang, R. Zou, M. Qian, X. Kong, E. Huo, X. Lin, L. Wang, X. Zhang, R. Ruan and H. Lei, Improvement of the carbon yield from biomass carbonization through sulfuric acid pre-dehydration at room temperature, *Bioresour. Technol.*, 2022, **355**, 127251.

50 M. J. Uddin, S. Liyanage, N. Abidi and H. S. Gill, Physical and Biochemical Characterization of Chemically Treated Pollen Shells for Potential Use in Oral Delivery of Therapeutics, *J. Pharm. Sci.*, 2018, **107**, 3047.

51 H. Wang, M. G. Potroz, J. A. Jackman, B. Khezri, T. Marić, N.-J. Cho and M. Pumera, Bioinspired Spiky Micromotors Based on Sporopollenin Exine Capsules, *Adv. Funct. Mater.*, 2017, **27**, 1702338.

52 J. M. Ageitos, S. Robla, L. Valverde-Fraga, M. Garcia-Fuentes and N. Csaba, Purification of Hollow Sporopollenin Microcapsules from Sunflower and Chamomile Pollen Grains, *Polymers*, 2021, **13**, 2094.

53 J. Li, W. Liu, X. Qiu, X. Zhao, Z. Chen, M. Yan, Z. Fang, Z. Li, Z. Tu and J. Huang, Lignin: a sustainable photothermal block for smart elastomers, *Green Chem.*, 2021, **4**, 823–836.

54 H. Song, Y. Ahmad Nor, M. Yu, Y. Yang, J. Zhang, H. Zhang, C. Xu, N. Mitter and C. Yu, Silica Nanopollens Enhance Adhesion for Long-Term Bacterial Inhibition, *J. Am. Chem. Soc.*, 2016, **138**, 6455.

55 J. Niu, C. Zhao, C. Liu, J. Ren and X. Qu, Bio-Inspired Bimetallic Enzyme Mimics as Bio-Orthogonal Catalysts for Enhanced Bacterial Capture and Inhibition, *Chem. Mater.*, 2021, **33**, 8052.

56 Y. Yang, X. Wu, L. Ma, C. He, S. Cao, Y. Long, J. Huang, R. D. Rodriguez, C. Cheng, C. Zhao and L. Qiu, Bioinspired Spiky Peroxidase–Mimics for Localized Bacterial Capture and Synergistic Catalytic Sterilization, *Adv. Mater.*, 2021, **33**, 2005477.

57 F. Cao, L. Zhang, H. Wang, Y. You, Y. Wang, N. Gao, J. Ren and X. Qu, Defect-Rich Adhesive Nanozymes as Efficient Antibiotics for Enhanced Bacterial Inhibition, *Angew. Chem., Int. Ed.*, 2019, **58**, 16236.

58 M. Hoop, Y. Shen, X.-Z. Chen, F. Mushtaq, L. M. Iuliano, M. S. Sakar, A. Petruska, M. J. Loessner, B. J. Nelson and

S. Pané, Magnetically Driven Silver–Coated Nanocoils for Efficient Bacterial Contact Killing, *Adv. Funct. Mater.*, 2015, **26**, 1063.

59 J. Shan, X. Li, K. Yang, W. Xiu, Q. Wen, Y. Zhang, L. Yuwen, L. Weng, Z. Teng and L. Wang, Efficient Bacteria Killing by Cu2WS4 Nanocrystals with Enzyme-like Properties and Bacteria-Binding Ability, *ACS Nano*, 2019, **13**, 13797.

60 R. Yang, G. Song, L. Wang, Z. Yang, J. Zhang, X. Zhang, S. Wang, L. Ding, N. Ren, A. Wang and X. Yu, Full Solar-Spectrum-Driven Antibacterial Therapy over Hierarchical Sn3O4/PDINH with Enhanced Photocatalytic Activity, *Small*, 2021, **17**, 2102744.

61 M. H. Beyki, S. E. Ganjbakhsh, S. Minaeian and F. Shemirani, Clean approach to synthesis of graphene like CuFe2O4@polysaccharide resin nanohybrid: Bifunctional compound for dye adsorption and bacterial capturing, *Carbohydr. Polym.*, 2017, **174**, 128–136.